



LAWRENCE  
LIVERMORE  
NATIONAL  
LABORATORY

# Investigation of B<sub>4</sub>C for Inhibiting Crystallization in Silica at High Temperatures

I. R. Crystal, B. J. Schauer, E. M. Sobalvarro  
Converse, J. T. Cahill, W. L. Du Frane, J. D.  
Kuntz, G. S. King

September 14, 2023

Ceramics International

## **Disclaimer**

---

This document was prepared as an account of work sponsored by an agency of the United States government. Neither the United States government nor Lawrence Livermore National Security, LLC, nor any of their employees makes any warranty, expressed or implied, or assumes any legal liability or responsibility for the accuracy, completeness, or usefulness of any information, apparatus, product, or process disclosed, or represents that its use would not infringe privately owned rights. Reference herein to any specific commercial product, process, or service by trade name, trademark, manufacturer, or otherwise does not necessarily constitute or imply its endorsement, recommendation, or favoring by the United States government or Lawrence Livermore National Security, LLC. The views and opinions of authors expressed herein do not necessarily state or reflect those of the United States government or Lawrence Livermore National Security, LLC, and shall not be used for advertising or product endorsement purposes.

# Investigation of B<sub>4</sub>C for inhibiting crystallization in silica at high temperatures

Isabel R. Crystal<sup>1,a</sup>, Ben Schauer<sup>1,a</sup>, Elizabeth Sobalvarro Converse<sup>a</sup>, James T. Cahill<sup>a</sup>, Wyatt L. Du Frane<sup>a</sup>, Gabriella King<sup>a,\*</sup>

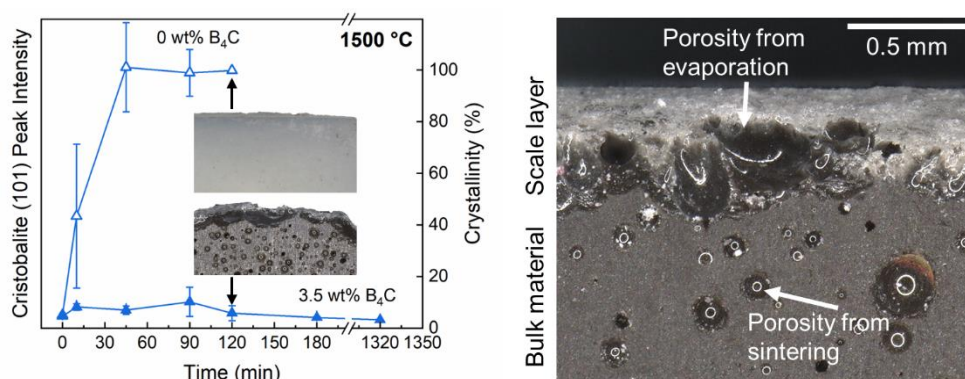
<sup>a</sup>Materials Science Division, Lawrence Livermore National Laboratory, Livermore, CA, 94550, USA

\*Corresponding author: [king112@llnl.gov](mailto:king112@llnl.gov)

<sup>1</sup>Isabel R. Crystal and Ben Schauer contributed equally to this article.

**Keywords:** Amorphous SiO<sub>2</sub>, Crystallization, X-ray diffraction, Thermal expansion

## Graphical Abstract:



## I. Abstract

Amorphous silica has numerous high temperature applications due to its inherent thermal shock resistance and low coefficient of thermal expansion (CTE). However, at the high temperatures required for processing ( $>1200$  °C), the metastable  $\beta$ -cristobalite phase preferentially forms and is accompanied by a volume change, and potential cracking, upon conversion to the low temperature  $\alpha$ -cristobalite phase. The CTE of the final crystalline phase is an order of magnitude higher than its amorphous counterpart. Here experimental results demonstrate that small additions of B<sub>4</sub>C (3.5 wt%) effectively inhibit silica crystallization in powder and sintered gel-cast forms up to 22 hours at temperatures as high as 1500 °C as confirmed via x-ray diffraction. The oxidation of B<sub>4</sub>C to B<sub>2</sub>O<sub>3</sub> and its subsequent melt and evaporation disrupts the nucleation and growth of the cristobalite phase. The mechanism for crystallization inhibition is further explored through optical microscopy to probe changes in surface morphology.

## II. Introduction

Amorphous silica (SiO<sub>2</sub>) has a wide range of industrial applications due to its thermal shock resistance, high dielectric strength, high adsorption capacity, ability to cool rapidly without crystallizing, low coefficient of thermal expansion (CTE), and optical properties. These properties enable the use of amorphous silica in applications such as telescope lenses, optical fibers, microchips, desiccants, and gels

for chromatography [1]. For higher temperatures, silica is used as a coating for various metal and alloy systems to protect from oxidation during service [2]–[4]. The low CTE and relatively high melting point of 1713 °C also make amorphous silica an ideal candidate for a variety of high temperature systems, especially multi-component systems where accommodating thermal mismatch is required. Morphological changes of materials during thermal cycling is an ongoing concern in high temperature multi-material applications [5]. Amorphous silica is known to undergo crystallization to the  $\beta$ -cristobalite phase in a matter of hours when exposed to high temperatures ( $> 1200$  °C) [6]. The developed  $\beta$ -cristobalite phase has a CTE an order of magnitude larger than that of amorphous silica (from  $5.5 \times 10^{-7} \text{ K}^{-1}$  to  $6 \times 10^{-6} \text{ K}^{-1}$ ), limiting the temperature range in which it can be used as a low CTE material [7]–[9]. In addition, when cooled below the range of 270–200 °C,  $\beta$ -cristobalite will undergo a phase change to  $\alpha$ -cristobalite [10]. This crystallographic change is accompanied by cracking due to a volume contraction of  $\sim 5\%$  and another increase in average bulk CTE to  $9.2 \times 10^{-5} \text{ K}^{-1}$  [9], [11].

There has been significant interest in amorphous silica with numerous studies focused on devitrification kinetics in efforts to prevent degradation of the unique thermal and optical properties that make amorphous silica desirable. The crystallization kinetics of silica has been well-studied in bulk glasses [6], [12], colloidal gel-derived powder [13], [14], and stock powder form [15]. In 1965, Richards and Wagstaff [12] noted the sensitivity of silica's crystallization to trace impurities. As such, the crystallization kinetics of silica in the presence of aluminum oxide, alkali metal oxides and salts, air moisture, and in air versus inert gas have been investigated with many impurities being observed to catalyze nucleation and thus crystallization [16], [17]. Certain dopants were found to inhibit rather than catalyze the cristobalite transformation, and this approach became acceptable for applications that did not require a high degree of purity. The addition of small amounts of binary boron compounds or rare earth elements has been shown to effectively reduce cristobalite formation during the sintering stage. Rare earth element oxides create local accumulation effects, raising the activation energy of molecular ordering, which prevents devitrification [18]. Many rare-earth oxides have been tested in low weight percent (1.5–2.5 wt%), including  $\text{Yb}_2\text{O}_3$ ,  $\text{Gd}_2\text{O}_3$  and  $\text{Ho}_2\text{O}_3$ , which have been shown to inhibit silica crystallization during processing at 1300 °C [19], [20]. However, there were clear signs of cristobalite development after sintering at 1400 and 1500 °C for 1–2 hours [20]. Furthermore, rare earth oxides are usually cost prohibitive, limiting scalability. By contrast, boron carbide ( $\text{B}_4\text{C}$ ) is relatively inexpensive. Incorporation of  $\text{B}_4\text{C}$  with as little as 3 wt% has been shown to inhibit crystallization over a range of sintering temperatures (1150–1400 °C) [21], [22]. The mechanism is based on the incorporation of network modifiers that disrupt  $\text{SiO}_2$  bond ordering [23]. Borides introduced into the network can form B-Si-O bonds, decreasing the density of uninterrupted O-Si-O bonds, which decreases the short-range order of the bond. The stability of the amorphous glass network is effectively increased by raising the activation energy of molecular rearrangement in the glass [18], [24].

Most investigations into these additives were generally limited to the study of powders and uniaxially pressed and sintered pellets [19]–[22], [24]. Cristobalite crystallization in undoped  $\text{SiO}_2$  was probed in injection molded silica-based ceramic cores by Kazemi et al. in 2013 [11] and in gel-cast components by Ali et al. in 2019 [25]. Later, Liu et al. [18] studied the effect of  $\text{Si}_3\text{N}_4$  additions in gel-cast silica components, but there are otherwise relatively few bodies of work dedicated to the investigation of crystallization kinetics in near-net shape components despite the tantalizing cost savings due to reduction in required machining for parts with increased complexity. Moreover, most devitrification studies are limited to the sintering stage, and thus the kinetics of crystallization in  $\text{SiO}_2$  are probed in temperatures and timescales relevant to processing (typically  $\leq 1300$  °C and less than 3 hours) rather than conditions encountered in applications. If  $\text{SiO}_2$  is to be incorporated into high temperature applications up

to 1500 °C with long exposure times relevant to these applications, it is necessary to develop an understanding of crystallization inhibition kinetics in such extreme environments. Liu et al. [18] investigated the crystallization kinetics of post-processed amorphous SiO<sub>2</sub> for applications in photovoltaics in the temperature range of 1300-1550 °C over the course of 10-240 minutes. While informative due to the probing of higher temperatures and hold times over 3 hours, the concern for photovoltaic conversion efficiency also narrowed the focus to silicon nitride as the sole dopant, which typically requires higher addition concentrations (greatest effectivity at 20 wt%) than B<sub>4</sub>C for a similar level of cristobalite suppression [18]. Thus, there is a need to understand the effect of dopants on crystallization in gel-cast components beyond the sintering stage as cristobalite formation typically determines the upper temperature limits and exposure times for applications requiring stable low CTE components.

In this work, the crystallization kinetics of post-sintered 3.5 wt% B<sub>4</sub>C-doped SiO<sub>2</sub> pucks prepared via gel casting were investigated. Samples were tested at high temperatures up to 1500 °C and relevant timescales spanning 0-180 minutes with a maximum time of 22 hours probed in a select sample. The extent of crystallization was probed qualitatively by comparing the X-Ray Diffraction (XRD) patterns collected for the series of times and temperatures assessed. Surface changes comprising of an apparent scale layer with bubbling and pitting were indicative of melting and were observed on samples tested > 120 minutes for temperatures ≥ 1400 °C. A relationship between this phenomenon and crystallization inhibition was established. Silica powders with the B<sub>4</sub>C additives were also used to study crystallization in a form factor with a higher surface area to volume ratio to verify the efficacy of B<sub>4</sub>C as an additive for inhibiting crystallization.

### III. Experimental

#### A. Materials & Methods

Amorphous silica cylinders were prepared via a negative additive manufacturing technique where a suspension is cast into a 3D printed mold as described by Rivera et al. [26] The process begins with printing the desired structures using a stereolithography printer (Form 3, Formlabs Inc.) and surrounding the print with a two-part silicone mix (Moldstar 30, Smooth-On Inc.) to create a negative. Once cured, the negative silicone mold can then be infilled by a ceramic slurry. The gel-casting suspension method reported by Wat et al. [27] is followed. Silicon dioxide powder (99.9%, 800 nm, spherical) manufactured by US Research Nanomaterials, Inc and boron carbide (< 5 μm) from ESK ceramics were the raw ceramic powders. Polyvinyl alcohol (PVA) (Molecular weight 13,000-23,000, 87-89% hydrolyzed, Aldrich) and 2,5-dimethoxy-2,5-dihydrofuran (DHF) (Sigma-Aldrich) were used as the monomer and cross-linker, respectively, with small volumes of concentrated HCl added to adjust the pH of the slurry to < 1.5 to catalyze breaking the conjugated DHF ring and initiate subsequent bonding/cross-linking to the PVA [28].

A planetary centrifugal mixer (ARE-310, Thinky) was used to incorporate all components of the aqueous solution for the gel-cast. Unless otherwise noted, all additions were followed by mixing at 1600-2000 RPM for 40-60 sec. First, PVA was mixed in deionized water where the water content was selected to control the final solids loading and the monomer content was fixed at 1.5 wt% (relative to the total powder). SiO<sub>2</sub> and B<sub>4</sub>C powders were added, and quantities were adjusted to prepare samples with 0 and 3.5 wt% B<sub>4</sub>C while maintaining a total solids loading of 50 vol% (SiO<sub>2</sub> plus B<sub>4</sub>C). Then, 1.0 wt% (relative to powder) DHF and 0.1 - 0.2g HCl were added to the mixture for cross-linking catalysis. The planetary

centrifugal mixer was also used at lower speeds (1300-1500 RPM) to mitigate air incorporation while casting the slurry (centrifugal assisted packing) into custom silicone molds designed to be compatible with 175mL Thinky containers. The slurry infilled the custom mold containing seven identical 7mm wide 5mm deep cylindrical holes and was dried in the mold for a minimum of 24 hours at room temperature with flowing air (fume hood) to allow sufficient time for the gelling reaction and moisture removal to occur. It is important to note that this negative additive manufacturing process can be generalized to fabrication of parts with increased complexity provided that the ceramic material can be suspended within the slurry.

After drying, the green bodies were demolded, and the binder was removed in a burnout step by heating samples for 2 hours at 500 °C (ramp rate of 10 °C/min) in atmospheric conditions using a three-zone quartz tube furnace (Applied Test Systems, Inc). Finally, samples were sintered under inert argon gas (ultra-high purity) in an alumina tube furnace (Lindberg/Blue M, Thermo Scientific) for 1 hour at 1200 °C or 1.5 hours at 1450 °C (ramp rate of 10 °C/min) for the 0 wt% and 3.5 wt% B<sub>4</sub>C samples, respectively. These conditions were selected to yield comparable densities because level of densification may affect the degree of surface nucleated crystallization [29]. Scanning electron microscopy (SEM, Apreo 2, ThermoFisher Scientific) verified the sintering conditions required for an acceptable level of densification (little to no open porosity) for both the 0 wt% and 3.5 wt% B<sub>4</sub>C samples. Densities of select sintered 0 wt% and 3.5 wt% B<sub>4</sub>C doped samples were also measured via Archimedes method. The average density and standard deviation (n=3) were 1.8±0.04 g cm<sup>-3</sup> for sintered 0 wt% B<sub>4</sub>C and 2.0±0.07 g cm<sup>-3</sup> for sintered 3.5 wt% B<sub>4</sub>C samples.

3.5 wt% B<sub>4</sub>C-doped silica powders were prepared to understand the efficacy of B<sub>4</sub>C additions in a system with a higher surface area in comparison to pellets. Doped powders were prepared by combining the appropriate amount of B<sub>4</sub>C and stock silica powder in a THINKY centrifuge cup and mixing at 2000 RPM for one minute in ~50 wt% ethanol. The mixed powder was dried in air overnight before testing. Fully crystalline silica powder was prepared in-house from amorphous stock powder for use as a reference and to provide context to the characteristic cristobalite (101) XRD peak intensity measurements of experimental samples. Crystalline powders were made by sintering stock US Research Nanomaterials, Inc silica powder for 24 hours at 1477 °C under inert argon gas in the Lindberg/Blue M alumina tube furnace.

Samples (gel-casts and powders) were placed in alumina crucibles and inserted into a pre-heated bottom loading furnace (RS reline of DT-31, Deltech) for different time intervals to explore the effect of time and temperature on crystallization for doped and undoped silica. Doped and undoped gel-cast samples were tested at 1300, 1400 and 1500 °C. For each temperature, hold times were systematically varied up to 3 hours (10, 45, 90, 120, 150, 180 minutes). An extended period of 22 hours was also tested at 1500 °C to exaggerate surface changes observed in samples held at shorter timescales. A set of three samples was tested for each temperature and time combination for error quantification in certain measurements. Powder mixes were only tested at 1400 °C for 90 minutes. This temperature and time were selected as they were known to lead to crystallization in undoped silica gel-casts, the desired point of comparison. Once the set temperature was reached, the stage was lowered, the sample(s) were quickly inserted, and the stage was raised. The sample loading procedure results in a temperature drop of 70-110 °C depending on the setpoint. To ensure approximate isothermal conditions, the hold time was not initiated until the target temperature was recovered to within 10 °C of the setpoint.

## B. Characterization

The heat-treated samples were characterized via x-ray diffraction (XRD, Bruker D8 Advance) to track crystallization as a function of time and temperature. XRD scans were conducted with Cu Ka

radiation source operating at 40 kV voltage and 40 mA current. To ensure appropriate resolution, the scanning step size was  $0.019^\circ$ , and the time per step was 0.0195 seconds for a total scan time per sample of 72 minutes. Both the external surface and interior cross-sections (low speed saw, Buehler IsoMet) were scanned to determine the extent of transformation. Samples were scanned over the range of  $2\theta = 10\text{--}80^\circ$  to monitor possible surface reactions from heat treatment as well as capture the peaks of  $\alpha$ -cristobalite, found at  $2\theta \approx 22.01^\circ, 28.48^\circ, 31.46^\circ$  and  $36.10^\circ$ , which correspond to the (101), (111), (102) and (200) reflections respectively [30]. **Figure 1** shows the crystalline XRD spectrum of a cristobalite reference sample, created by sintering stock silica powder at  $1477^\circ\text{C}$  for 24 hours. **Figure 1b** is the spectrum of an amorphous control sample made from stock powder.  $\text{SiO}_2$  phase markers are shown for the low temperature  $\alpha$ -cristobalite tetragonal structure with  $P4_12_12$  space group [31].  $\alpha$ -cristobalite has its most intense peak at  $2\theta \approx 22.01^\circ$ , while amorphous silica has no sharp peaks in XRD [30]. Note, all XRD patterns are reported as raw data without subtracting the background signal. While samples were tested in triplicate, a single representative XRD pattern was selected from the set for each condition summarized within the figures.

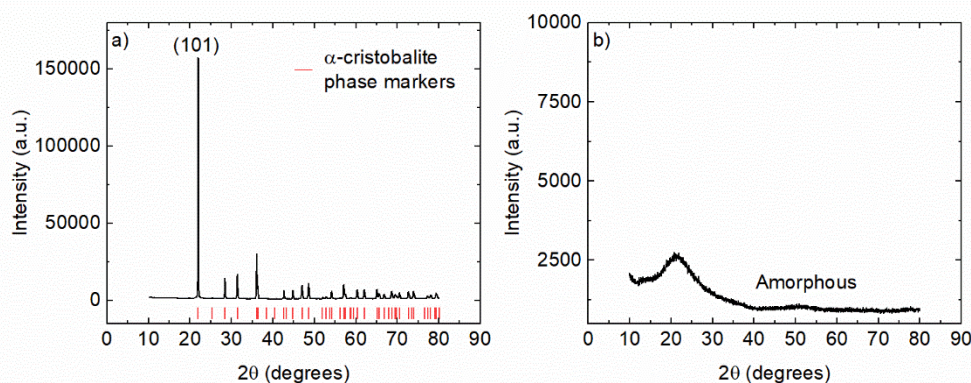


**Figure 1.** X-ray diffraction pattern for a) fully crystalline (100 wt% cristobalite) powders and b) fully amorphous (0 wt% cristobalite) powders with relevant phase markers.

A digital microscope (VHX-7100, Keyence corporation) and ImageJ software were used in tandem to characterize any surface level microstructural changes that occurred with the isothermal exposure. As some samples were observed to develop a scale layer, the thickness of this evolved layer was quantitatively measured via an external ImageJ macro for measuring the distance between user-defined segmented lines. The macro automatically constructs 15 random lines between the two user-defined lines (such that they are orthogonal to the bottom line) and computes an average and standard deviation in units of pixels [32]. For these measurements, 15 randomly generated measurement lines were used to yield an average film thickness and standard deviation. An example of the macro output is contained in the supplementary material (**Figure S1**). To determine the error associated with the measurement technique, the process was repeated for the same image three times, and the standard error of the mean was less than  $\sim 10\ \mu\text{m}$ . To determine the spread in the data, the macro was applied to three images collected from different regions within a given sample. Using the three different images, a weighted mean and weighted standard deviation can be calculated. Similarly, while samples were tested in triplicate, only a single representative sample from the set was analyzed for the microstructural changes.

## IV. Results and Discussion

## A. Crystallization Inhibition and Kinetics

The 0 wt% B<sub>4</sub>C control gel cast samples were exposed to temperatures of 1300, 1400, and 1500 °C for 10 to 120 minutes, while the 3.5 wt% B<sub>4</sub>C samples were subjected to the same isothermal temperatures for 10 to 180 minutes. Following the isothermal treatment, the surfaces of the samples were characterized by XRD. As there are a number of studies that correlate the intensity of the (101) cristobalite peak with the fraction transformed, trends in the change in peak intensity can be used to discuss trends in crystallization [18], [33]. Similar comparisons of XRD patterns for the 0 wt% B<sub>4</sub>C samples to the 3.5 wt% B<sub>4</sub>C samples reveal that there was significantly less cristobalite crystallization after 120 minutes of isothermal treatment at each of the three temperatures, as evidenced by lower intensity (101) peaks (**Figure 2**) [18], [34]. In general, the 0 wt% B<sub>4</sub>C sample sets treated at 1300 °C crystallized minimally across all hold times probed (10-120 minutes). The exception was one sample held at 90 minutes which increased the average measured peak intensity for the set to 11,000 a.u. and is responsible for the significant variance in the set as observed through a difference in intensity of ±10,000 a.u.. After 120 minutes at 1300 °C, the 0 wt% B<sub>4</sub>C control showed a small extent of crystallization with an intensity of the (101) peak of approximately 5000 a.u. (**Figure 2**Error! Reference source not found.a). For a fixed isothermal hold time (120 minutes), the (101) peak increased by more than 15x as the isothermal temperature was raised from 1300 °C to 1400 °C (**Figure 2**Error! Reference source not found.a,b). Between the 1400 °C and 1500 °C samples, there was less than a 10% increase in (101) peak intensity (**Figure 2**b,c), indicating that both isothermal temperatures greater than 1300 °C result in a high degree of crystallization.

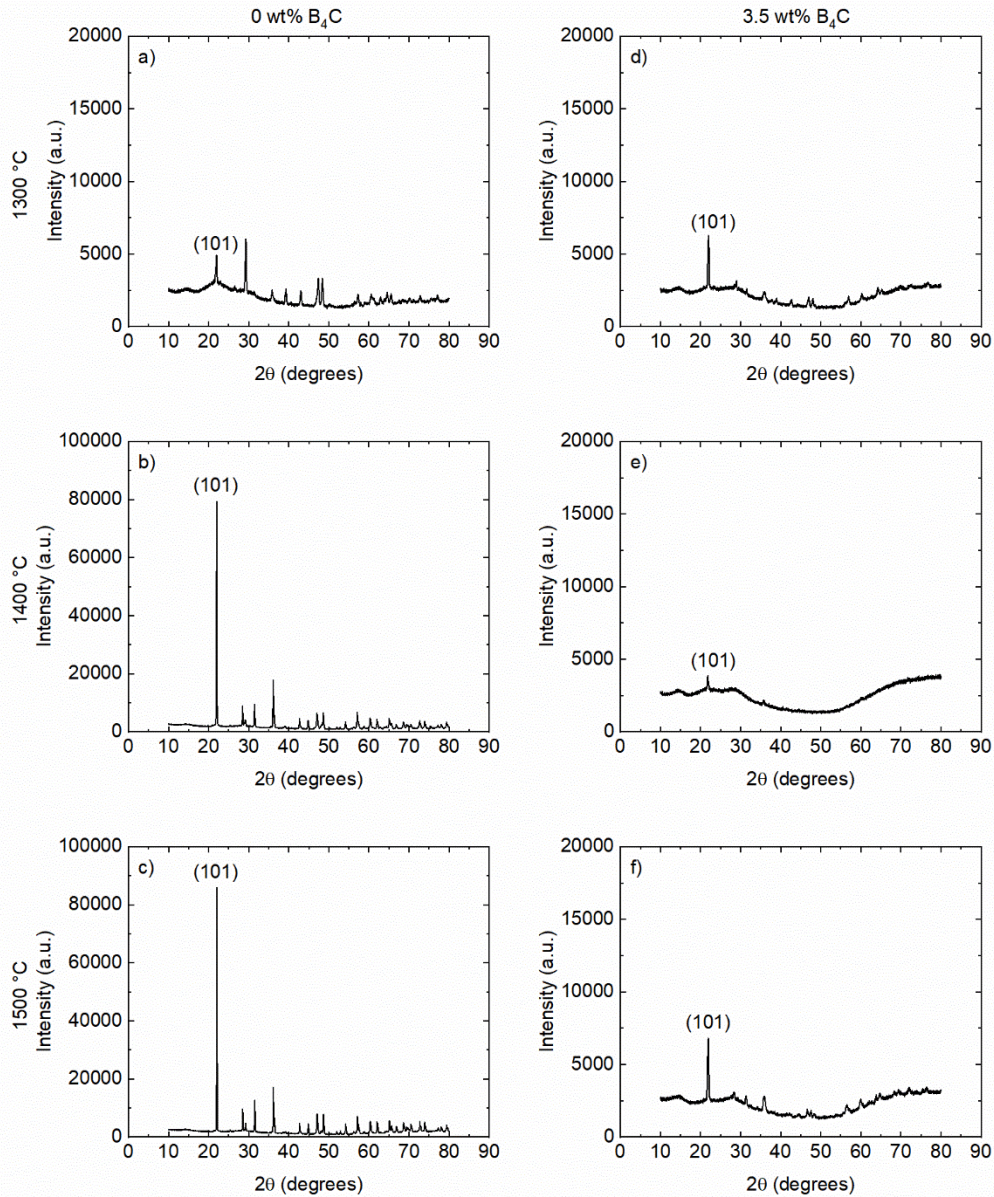


**Figure 2.** X-ray diffraction patterns collected after 120 minute exposure time for 0 wt% B<sub>4</sub>C control sample treated at a) 1300 °C, b) 1400 °C, c) 1500 °C and for 3.5 wt% B<sub>4</sub>C doped gel-cast monoliths after heated treatment at d) 1300 °C, e) 1400 °C, and f) 1500 °C with the characteristic (101) peak labeled.

The rate of increase of the measured (101) peak intensity is related to the rate of crystallization [29]. Thus, the average peak intensity extracted for each time and temperature combination are compared (**Figure 3**). For ease of discussion, the intensities reported are also correlated to a percent crystallinity by normalizing the intensities by the average value measured for 1500 °C between 45 and 120 minutes, which are assumed to be fully crystalline across all three exposure times (**Figure 3**). To avoid presenting repetitive data, the average intensity for the as-sintered samples for the 0 and 3.5 wt% B<sub>4</sub>C series is only included in the dataset for 1500 °C isothermal curves. However, as these samples did not show any discernable (101) peak, the extracted intensities corresponding to the  $2\theta \approx 22.01^\circ$  value is merely a

measurement of the amorphous hump where the reported standard deviation reflects the measurement noise.

The 0 wt% B<sub>4</sub>C samples held at temperatures higher than 1300 °C followed the expected crystallization rate and crystallized quickly. For the same hold time, higher levels of crystallization were measured for samples held at 1500 °C as compared to 1400 °C (**Figure 3**). The (101) peak intensities extracted for the 1500 °C dataset for the undoped material show the greatest rate of increase in the 0-to-10-minute rate with a change of ~33,000 a.u.. After 45 minutes of exposure at 1500 °C, the average (101) peak intensity appears to reach a plateau. For the 1400 °C isothermal condition, the rate of increase for the measured (101) peak intensity is reduced after 45 minutes of exposure with the largest increase of the average intensity value (~42,000 a.u.) reported from 10-to-45 minutes followed by a much smaller change (~5,000 a.u.) over the 45-to 90-minute range. While the intensities extracted for the 1400 °C samples continue to increase at a more gradual rate, the (101) peak measured at 180 minutes is comparable to that reported for the 1500 °C sample set with less than a 2,000 a.u. difference. This trend, coupled with the decrease in rate of increase of the intensity for the 1400 °C series, could suggest a possible plateau and convergence of these two data sets if longer hold times were probed. The noted increase in the crystallization rate followed by a gradual decrease in transformation is consistent with literature on nucleation and growth [6], [29], [35]. It is widely established that the isothermal kinetics of a range of materials can be described by the Avrami equation, where the extent of transformation as a function of time has a sigmoidal form [18], [36]. Initially, the reaction rate is small as an induction period is required to initiate nucleation of crystallites. Then the rate increases to a maximum at the point of inflection and finally decreases to zero or plateaus when the transformation is complete. Given the approximate plateau in intensity for the 1500 °C and the high rate of crystallization that is expected at the inflection point of the theoretical sigmoidal curve, it makes sense that the error bars are so high for the 10 minute hold time as the samples would be sensitive to slight deviations in thermal gradients within the furnace at this point. The time intervals selected appear to miss the approximate point of inflection and greatest crystallization rate for the 1400 °C series, which leads to small standard deviations.

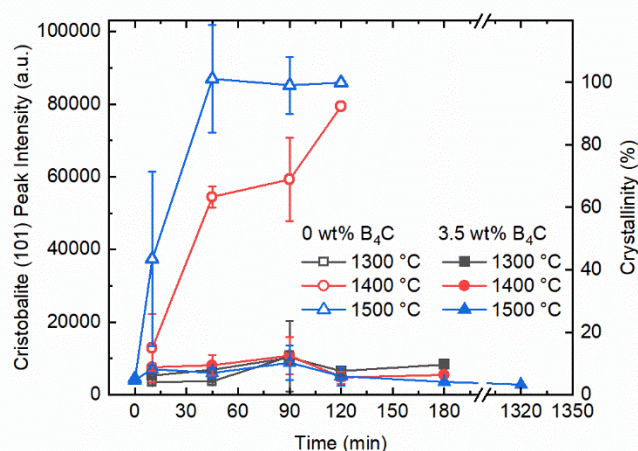


**Figure 3.** Relative Intensity of the characteristic (101) peak extracted from x-ray diffraction patterns collected, and corresponding percent crystallinities, for 3.5 wt% B<sub>4</sub>C-doped and 0 wt% B<sub>4</sub>C (undoped) gel-cast samples with different isothermal treatments. Error bars are not present on the 120-minute data points as these samples were not run in triplicate.

Doping SiO<sub>2</sub> with 3.5 wt% B<sub>4</sub>C proved to be an effective method for inhibiting crystallization in post-processed silica samples, even at high temperatures and long hold times. The XRD patterns for samples with 0 wt% and 3.5 wt% B<sub>4</sub>C subjected to the 1300 °C at 120 minutes reveal comparably low levels of (101) peak development (**Figure 2a,d**). At temperatures above 1300 °C the differences in the crystallinity of the 0 wt% and 3.5 wt% become more apparent. For the 1400 °C treatment at 120 minutes, the 3.5 wt% sample exhibits a (101) peak intensity that is similar to the intensity measured at 1300 °C (**Figure 2b,e**), which is approximately 10x lower than the value for the 0 wt% B<sub>4</sub>C counterpart. After the 1500 °C isothermal treatment, the 3.5 wt% B<sub>4</sub>C sample continues to display a (101) peak intensity that is consistent with that measured for lower isothermal temperatures (~5,000 a.u.) while the 0 wt% B<sub>4</sub>C sample shows about a 17x higher intensity (**Figure 2c,f**). The addition of the dopant is so robust that the curves presented in **Figure 3** for the extracted average intensities from the three different isothermal treatments are overlaid. Here, it is apparent that the (101) peak intensities are all relatively stable except for a small uptick in value with the maximum of each set consistently occurring at 90 minutes followed by a decrease back to a stable value at times >90 minutes. However, the changes in intensity are quite small and all within the measured deviation of the 3.5 wt% B<sub>4</sub>C dataset for each isothermal condition.

To determine the limitations of the B<sub>4</sub>C dopant, a select sample was held for 22 hours at 1500 °C. XRD confirmed that even after this extreme treatment, the sample remained amorphous (**Figure 4**). This result is significant as few studies of this nature have probed hold times longer than a few hours. While the extracted intensity was still included in **Figure 3**, it is important to note that the extreme conditions induced morphological surface evolution treatment that left the exterior surface uneven as observed via optical microscopy (**Figure S1**). Thus, there is the possibility of some peak shifting in the XRD pattern collected for this time and temperature condition. 3.5 wt% B<sub>4</sub>C-SiO<sub>2</sub> powder mixes were also subjected to isothermal treatment as a means of separating the selected sample geometry / form from the level of inhibition. The doped powder mixes were treated for 90 minutes at 1400 °C and maintained the amorphous phase with no characteristic cristobalite peak development (**Figure S2**). The 0 wt% B<sub>4</sub>C-SiO<sub>2</sub> powders subjected to the same conditions showed significantly higher levels of cristobalite formation, developing a (101) peak of approximately 20,000 a.u. (**Figure S2**).

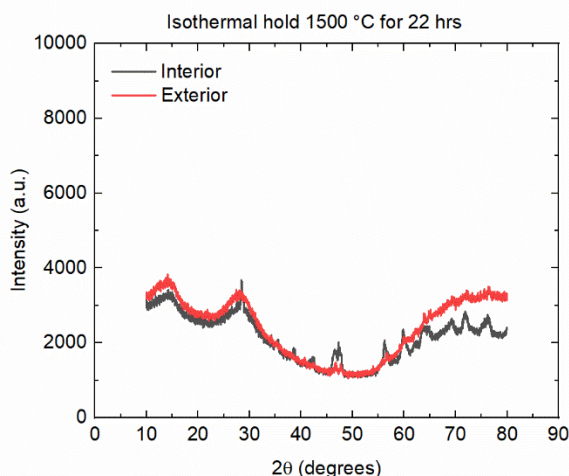


**Figure 4.** Comparison of X-ray diffraction patterns for the exterior surface and interior cross-section of the 3.5 wt% B<sub>4</sub>C samples subjected to heat treatment of 22 hours at 1500 °C.

This quantification of transformation and crystallization kinetics often involves incorporating an internal standard to calibrate the degree of transformation as a function of time to extract an activation energy for the transformation [29]. However, this process would require powder samples, while the purpose of this study was to focus on B<sub>4</sub>C as an additive for inhibiting crystallization in gel-cast SiO<sub>2</sub> parts. Activation energy of transformation may also be calculated with the use of an external reference curve [18], but this analysis was not possible as the probed conditions were unable to induce enough crystallization to have the data spread that is requisite for the calculation. The extracted intensity of the XRD patterns collected for the bulk monoliths can therefore be used to indicate an increase of fraction transformed but cannot be objectively quantified. Additionally, such a study would still not fully represent the surface crystallization.

## B. Surface Crystallization

Given that all samples are loaded at temperature in a furnace at atmospheric conditions, the heat treatment is accompanied by oxidation of the B<sub>4</sub>C material at the surface of the gel-cast part. B<sub>4</sub>C has been shown to oxidize into B<sub>2</sub>O<sub>3</sub> and melt, creating a protective layer that prevents further oxidation of the underlying material [37], [38]. The oxidation kinetics of B<sub>4</sub>C powder have been reported to be highly dependent on the particle size, with the onset of oxidation at approximately ~500°C and a significant increase in rate at approximately ~650°C [39]. Gogotsi and Lavrenko et al. [40]–[43] investigated oxidation in sintered hot-pressed B<sub>4</sub>C and noted the formation of a thin transparent film of B<sub>2</sub>O<sub>3</sub> that cracked with cooling, which is consistent with the formation of the brittle scale observed in the 3.5 wt% B<sub>4</sub>C-doped SiO<sub>2</sub>. The developed surface scale layer was further investigated through both XRD of interior cross-sections and optical microscopy techniques.

The cristobalite phase is known to preferentially form at the surface as well as impurity sites [14], [29], [35], [44]. The XRD results presented in Results and Discussion: Section A were all collected at the surface. XRD analysis of the interior bulk is particularly important due to the amorphous nature of the formed B<sub>2</sub>O<sub>3</sub> layer at the surface which can potentially hide any evolved cristobalite. Thus, to compare the extent of crystallization of the exterior surface and the interior, cross-sections were prepared by cutting the gel-cast components in half and measuring the exposed cross section by XRD (**Figure 5**). After treatment at 1400 °C for 90 minutes, the 0 wt% B<sub>4</sub>C control sample exhibited nearly full crystallization at the surface (**Figure 5a**), while the cross-section revealed an amorphous curve with a low intensity (101) peak (**Figure 5b**). The 3.5 wt% B<sub>4</sub>C sample shows a perceptible decrease of approximately 3,000 a.u. in the (101) peak intensity between the exterior (**Figure 5c**) and the interior cross-section (**Figure 5d**). This difference in crystallinity is less than that for the 0 wt% B<sub>4</sub>C sample because the 3.5 wt% B<sub>4</sub>C sample has a low intensity (101) peak at the surface. Even in the most extreme test case of 1500 °C for 22 hours, the exterior surface scan and interior cross-sections were shown to be comparable (**Figure 4**). XRD analysis demonstrated that both the surface scale and interior remain largely amorphous after 22 hours with no strong (101) cristobalite peak formed. However, a small (111) peak was observed for the interior scan which can potentially be due to peak shifting from the uneven surface or contamination. It is also possible that this peak can be attributed to a combination of a portion of the surface and bulk being scanned as the sample was brittle after the long exposure, which made cross-sectioning difficult.

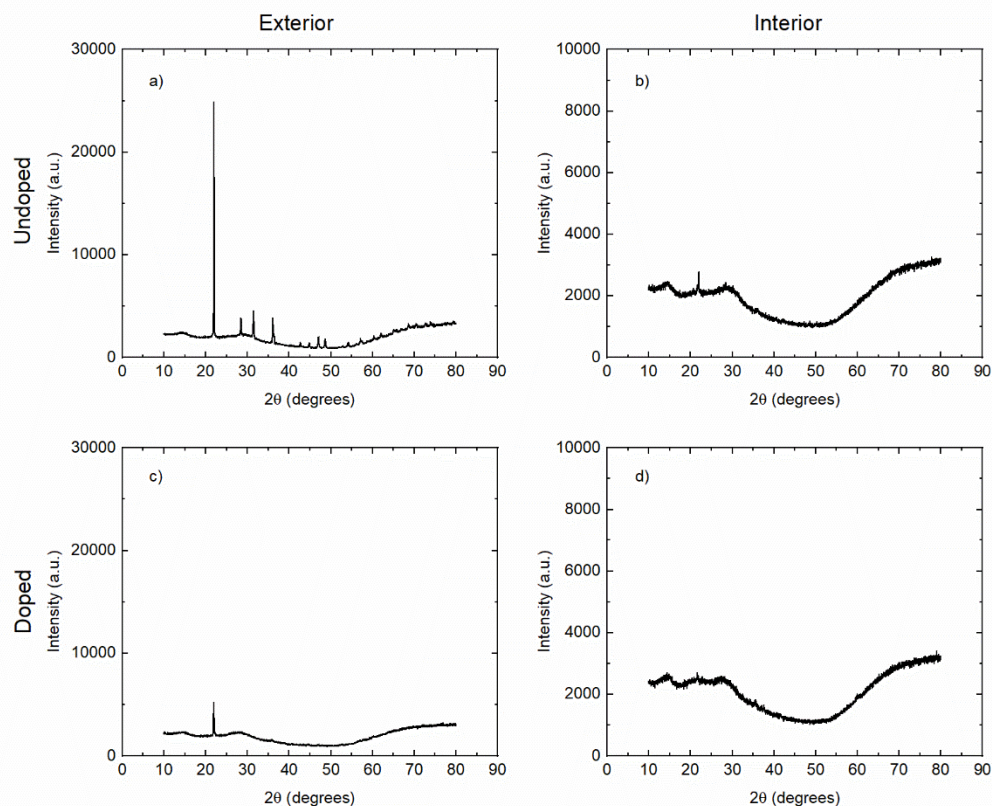


**Figure 5.** X-ray diffraction patterns for 0 wt% B<sub>4</sub>C silica control sample collected for the a) exterior surface and b) interior cross-section and 3.5 wt% B<sub>4</sub>C doped samples scanned at the c) exterior surface and d) interior cross-section. Both samples were heat treated for 90 minutes at 1400 °C.

Crystallization is sensitive to several parameters including density, site impurities/contamination, and defect concentration. In particular, impurities could come from the silicone molds during casting, fume hood during drying, or furnaces during calcination. While the data was consistent between sets, some outliers may be attributed to slight variations in densities due to thermal gradients during processing and the potential incorporation of impurities leading to higher levels of preferential cristobalite nucleation.

### C. Surface Evolution with Isothermal Heating

Morphological evolution with crystallization was characterized through optical microscopy of the sample surface and interior cross-sections. Note that for the series of figures discussed in this section, a unique sample was imaged for each temperature and time combination. However, the top-down view and cross-section pairs were collected using the same specimen. When the isothermal treatment was complete, samples were quickly removed from the furnace at temperature. Thus, the samples were effectively quenched, and any evolution in the surface/bulk is locked into the structure and can be examined via microscopy. The 0 wt% B<sub>4</sub>C samples were visually consistent across all isothermal treatments. After treatment at 1500 °C, there were no apparent changes to the surface or bulk (**Figure S3**) with no obvious differences noted between the exterior and interior cross-section. Without the presence of B<sub>4</sub>C, or any oxidizing species, the sample does not form a protective scale, and the nucleation and growth of the

crystalline phase is almost immediate and rapidly increases with time. Similarly, the 3.5 wt% B<sub>4</sub>C subjected to the 1300 °C treatment showed no physical changes (**Figure S4**).

For higher temperatures, the 3.5 wt% B<sub>4</sub>C samples showed high levels of cristobalite suppression following exposure to higher isothermal temperatures as shown by XRD, but these treatments were accompanied by visual changes to the surface. The onset of scale development from the oxidation of B<sub>4</sub>C into B<sub>2</sub>O<sub>3</sub>(l) and subsequent vaporization with bubble formation and pitting from their collapse, is readily observed in the quenched parts after 120 minutes at 1400°C (**Figure 6**). The scale formation and observed presence of the highly porous surface from the collapsed gas bubbles worsens with increasing hold time (**Figure 6**). For a higher treatment temperature, physical changes are exhibited after shorter time intervals. 3.5 wt% B<sub>4</sub>C samples that were held for 60 minutes at 1500°C exhibited surface pitting and sagging and developed a partially opaque, white exterior scale (**Figure 7**).

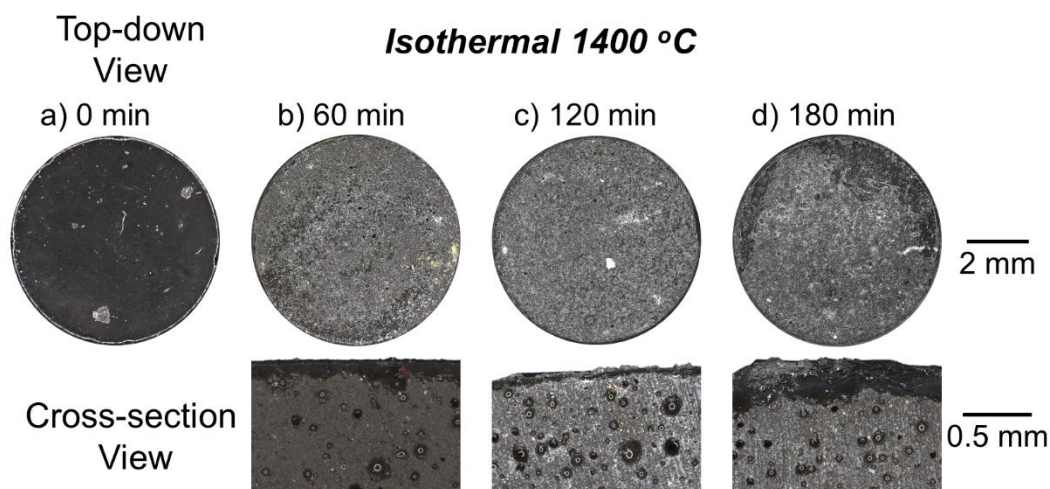


**Figure 6.** Optical microscopy of 3.5 wt% B<sub>4</sub>C doped gel-cast components top-down view and cross-sections at different times for the 1400 °C isothermal treatment where each time/ temperature combination is represented by a unique sample. The following treatments are imaged: a) 0 min, b) 60 min, c) 120 min, and d) 180 min at 1400 °C.

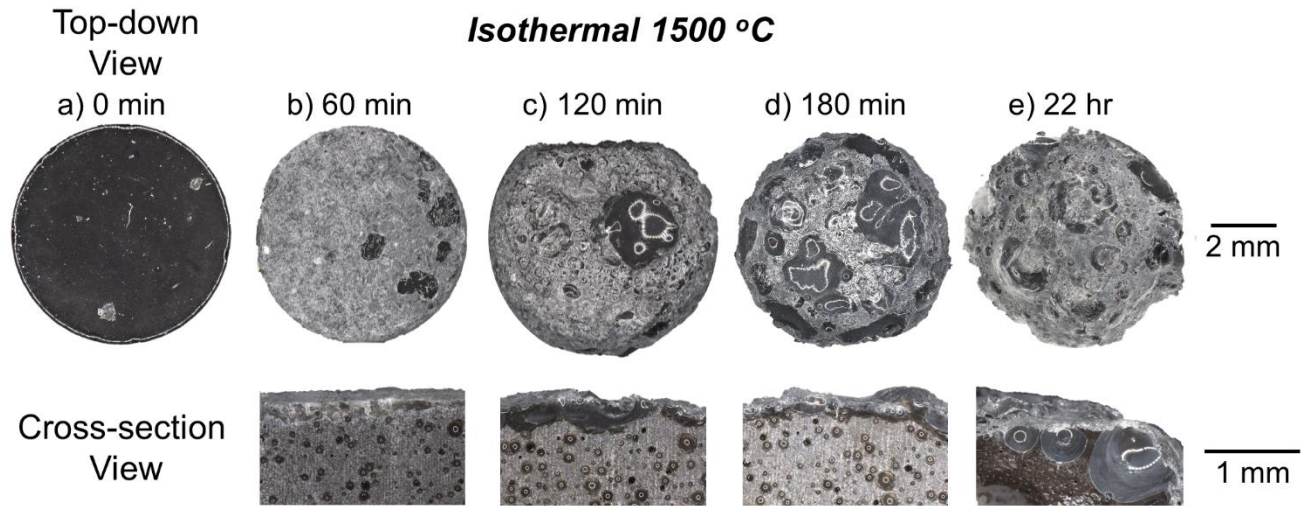


**Figure 7.** Optical microscopy of 3.5 wt% B<sub>4</sub>C doped gel-cast components top-down view and cross-sections at different times for the 1500 °C isothermal treatment where each time/ temperature combination is represented by a unique sample. The following treatments are imaged: a) 0 min, b) 60 min, c) 120 min, d) 180 min, and e) 22 hours at 1500 °C.

Scale layer thickness was extracted from optical microscopy of cross-sections using ImageJ for image processing. The image processing macro required user identification of the external boundary of the surface scale and the interface between the formed scale and interior material. As the scale layer thickness was found to vary locally and depends on the presence of bubbles or pores, three representative sections were chosen for measurement for each time and temperature combination. The resulting weighted mean and standard deviation for the surface layer thickness demonstrate the progression of the scale formation over time (**Figure 8**). No scale was developed in the 0 wt% and the 3.5 wt% B<sub>4</sub>C samples held at 1300 °C. At higher temperatures, the scale first forms as a thin matte gray surface coating, in contrast to the typical shiny black finish present on doped samples before heat treatment. It appears that the scale formation is a time dependent process, with the onset of formation shifting with the isothermal temperature. For 1400 °C, the scale is evident at times greater than 60 minutes whereas after only 45 minutes at 1500 °C, an average scale layer of ~70 μm is already apparent. Thus, for all times measured, the samples treated at 1500 °C exhibited a thicker scale layer compared to those exposed to 1300 and 1400 °C.

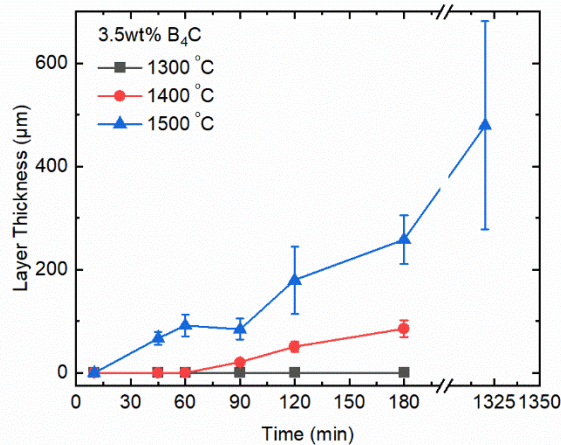


**Figure 8.** The thickness of the affected oxidized layer extracted via image processing of optical microscopy of cross-sections for 3.5 wt% B<sub>4</sub>C-doped samples subjected to various isothermal treatments.

In general, both the weighted mean of scale layer thickness and the weighted standard deviation were found to increase with time (**Figure 8**). The trend in the standard deviation is consistent with the onset of bubbling, which significantly increases the thickness of the affected layer close to the bubble, as these features are locked into the quenched material. Select samples were subjected to more aggressive isothermal hold times to further investigate scale development as well as to assess crystallization present on the surface and in the bulk at the extreme. The rate of the scale thickness (slope of the layer thickness vs time curve) increased predominantly during the time span of the first 1.5 to 3 hours for samples held at 1500 °C, with a more than 300% increase in scale layer thickness. From 3 to 22 hours, however, the sample only exhibited an 85% increase in scale thickness accompanied by a much larger standard deviation.

During isothermal treatment, the B<sub>4</sub>C at the surface is converted to oxidized B<sub>2</sub>O<sub>3</sub>. The B<sub>2</sub>O<sub>3</sub> product will progressively melt and form a glassy film on the surface which slows the progression of the oxidation reaction. At increased isothermal temperatures and hold times, the present liquid B<sub>2</sub>O<sub>3</sub> at the surface can evaporate, creating gaseous/bubbling sites that can expand to have a greater diameter than the porosity inherently present due to the sintering process (**Figure 7d, e**). The largest bubbles often collapse, creating pitting on the surface of samples held for over 2 hours. Vaporization at a rate high enough to cause large bubbling is possible because of B<sub>2</sub>O<sub>3</sub>'s vapor pressure, which is among the highest of oxides: ~344 Pa at 1527 °C [45]. B<sub>2</sub>O<sub>3</sub> will vaporize around 1100 °C, similar in temperature to the point at which its precursor is oxidizing [46]. Tripp and Graham [45], [47] plotted the relationship between B<sub>2</sub>O<sub>3</sub> vaporization rate and temperature and found that B<sub>2</sub>O<sub>3</sub> vaporized at a relatively high rate of 0.08 (mg/cm<sup>2</sup>)<sup>2</sup>/min at 1400 °C – more than twice the rate at measured at 1300 °C for the same conditions (P<sub>O<sub>2</sub></sub> = 3.3 x 10<sup>-4</sup> Pa). B<sub>2</sub>O<sub>3</sub> scale formation may protect the silica beneath it from crystallization by shielding it from atmospheric oxygen, and by interrupting the crystallization surface nucleation process. This hypothesis is consistent with the measured scale layer thickness as the growth rate was found to increase with temperature, with the highest rate approximately coinciding with the evaporation of B<sub>2</sub>O<sub>3</sub> and the formation of the large bubbles (**Figure 8**). The formation and collapse of gaseous B<sub>2</sub>O<sub>3</sub> bubbles in the scale layer results in a much larger standard deviation in measured layer thickness for samples held at 1500 °C.

## V. Conclusions

The extent of cristobalite inhibition was probed in sintered bulk gel-cast components that were subjected to various isothermal treatments. XRD determined that the undoped 0 wt% B<sub>4</sub>C samples exhibited high levels of crystallization across the majority of treatments and the extent of transformation was correlated to the increase in the (101) peak intensity. In comparison, the 3.5 wt% B<sub>4</sub>C gel-cast samples exhibited negligible amounts of transformation with very low (101) peak intensity measured across all assessed isothermal temperatures and holds. A maximum of 22 hours at 1500 °C was tested which is a significant result as, to our knowledge, is among the longest isothermal holds probed for a devitrification study and therefore demonstrates how robust the dopant system is for inhibiting cristobalite.

Evolution in the surface morphology was also studied through optical microscopy of the gel-cast components and cross-sections. A scale layer with bubbling through the thickness was observed to form in the 3.5 wt% B<sub>4</sub>C samples subject to 1400 °C and 1500 °C isothermal treatment which is consistent with evolution of the oxidation product B<sub>2</sub>O<sub>3</sub> from liquid to vapor state. The presence of the scale likely acts to disrupt the nucleation and growth of cristobalite at the surface while creating a protective layer that restricts the mobility of oxygen to the interior material. The results demonstrate that 3.5 wt% B<sub>4</sub>C dopant can be used for inhibiting crystallization in conditions and sample geometries that are representative conditions required for applications. While the addition of B<sub>4</sub>C was indeed effective for inhibiting crystallization, further characterization of the scale is required to determine how the varied surface evolution will impact formulation efficacy as a low CTE material for high temperature applications.

## VI. Acknowledgements

This work was performed under the auspices of the U.S. Department of Energy by Lawrence Livermore National Laboratory under Contract DE-AC52-07NA27344. Released under LLNL-JRNL-854285.

This research was developed with funding from the Defense Advanced Research Projects Agency (DARPA). The views, opinions and/or findings expressed are those of the authors and should not be interpreted as representing the official views or policies of the Department of Defense or the U.S. Government. Distribution A: Approved for Public Release, Distribution Unlimited.

## VII. Appendix A. Supplementary Material

See supplementary material document

## VIII. References

- [1] A. N. Saxena, *Invention of Integrated Circuits: Untold Important Facts*. in International Series on Advances in Solid State Electronics and Technology. World Scientific Publishing Co. Pte. Ltd., 2009.
- [2] C. Yu, S. Zhu, D. Wei, and F. Wang, "Amorphous sol-gel SiO<sub>2</sub> film for protection of Ti<sub>6</sub>Al<sub>4</sub>V alloy against high temperature oxidation," *Surf. Coat. Technol.*, vol. 201, no. 12, pp. 5967–5972, Mar. 2007, doi: 10.1016/j.surfcoat.2006.11.004.

- [3] A. Atkinson and J. W. Gardner, "The diffusion of  $\text{Fe}^{3+}$  in amorphous  $\text{SiO}_2$  and the protective properties of  $\text{SiO}_2$  layers," *Corros. Sci.*, vol. 21, no. 1, pp. 49–58, Jan. 1981, doi: 10.1016/0010-938X(81)90063-9.
- [4] K. S. Coley, A. T. Tuson, S. R. J. Saunders, M. J. Bennett, and C. F. Knights, "On the stability of amorphous silica coatings for high-temperature service," *Mater. Sci. Eng. A*, vol. 120–121, pp. 461–466, Dec. 1989, doi: 10.1016/0921-5093(89)90802-2.
- [5] N. P. Padture, M. Gell, and E. H. Jordan, "Thermal barrier coatings for gas-turbine engine applications," *Science*, vol. 296, no. 5566, pp. 280–284, Apr. 2002, doi: 10.1126/science.1068609.
- [6] N. G. Ainslie, C. R. Morelock, and D. Turnbull, "Devitrification kinetics of fused silica," in *Symposium on Nucleation and Crystallization in Glasses and Melts*, Columbus, OH, 1962, pp. 97–107.
- [7] N. S. Jacobson, D. S. Fox, J. L. Smialek, E. J. Opila, C. Dellacorte, and K. N. Lee, "Performance of ceramics in severe environments," in *ASM Handbook Corrosion: Materials*, vol. 13B, 2005. Accessed: Sep. 13, 2023. [Online]. Available: <https://dl.asminternational.org/handbooks/edited-volume/25/chapter/344053/Performance-of-Ceramics-in-Severe-Environments>
- [8] M. Cavillon, P. D. Dragic, and J. Ballato, "Additivity of the coefficient of thermal expansion in silicate optical fibers," *Opt. Lett.*, vol. 42, no. 18, pp. 3650–3653, Sep. 2017, doi: 10.1364/OL.42.003650.
- [9] M. Dapiaggi, L. Pagliari, A. Pavese, L. Sciascia, M. Merli, and F. Francescon, "The formation of silica high temperature polymorphs from quartz: Influence of grain size and mineralising agents," *J. Eur. Ceram. Soc.*, vol. 35, no. 16, pp. 4547–4555, Dec. 2015, doi: 10.1016/j.jeurceramsoc.2015.08.015.
- [10] D. M. Hatch and S. Ghose, "The  $\alpha$ - $\beta$  phase transition in cristobalite,  $\text{SiO}_2$ ," *Phys. Chem. Miner.*, vol. 17, no. 6, pp. 554–562, Feb. 1991, doi: 10.1007/BF00202234.
- [11] A. Kazemi, M. A. Faghihi-Sani, and H. R. Alizadeh, "Investigation on cristobalite crystallization in silica-based ceramic cores for investment casting," *J. Eur. Ceram. Soc.*, vol. 33, no. 15, pp. 3397–3402, Dec. 2013, doi: 10.1016/j.jeurceramsoc.2013.06.025.
- [12] F. E. Wagstaff and K. J. Richards, "Preparation and Crystallization Behavior of Oxygen-Deficient Vitreous Silica," *J. Am. Ceram. Soc.*, vol. 48, no. 7, pp. 382–383, 1965, doi: 10.1111/j.1151-2916.1965.tb14767.x.
- [13] C.-H. Chao and H.-Y. Lu, "Crystallization of  $\text{Na}_2\text{O}$ -doped colloidal gel-derived silica," *Mater. Sci. Eng. A*, vol. 282, no. 1, pp. 123–130, Apr. 2000, doi: 10.1016/S0921-5093(99)00758-3.
- [14] A. G. Verduch, "Kinetics of Cristobalite Formation from Silicic Acid," *J. Am. Ceram. Soc.*, vol. 41, no. 11, pp. 427–432, 1958, doi: 10.1111/j.1151-2916.1958.tb12890.x.
- [15] L.-Y. Wang and M.-H. Hon, "The effect of cristobalite seed on the crystallization of fused silica based ceramic core — A kinetic study," *Ceram. Int.*, vol. 21, no. 3, pp. 187–193, Jan. 1995, doi: 10.1016/0272-8842(95)90909-3.
- [16] X. Li, X. Yin, L. Zhang, and S. He, "The devitrification kinetics of silica powder heat-treated in different conditions," *J. Non-Cryst. Solids*, vol. 354, no. 28, pp. 3254–3259, Jun. 2008, doi: 10.1016/j.jnoncrsol.2008.02.016.
- [17] P. P. Bihuniak, "Effect of Trace Impurities on Devitrification of Vitreous Silica," *J. Am. Ceram. Soc.*, vol. 66, no. 10, pp. c188–c189, 1983, doi: 10.1111/j.1151-2916.1983.tb10549.x.
- [18] J. Liu *et al.*, "Inhibiting crystallization of fused silica ceramic at high temperature with addition of  $\alpha$ - $\text{Si}_3\text{N}_4$ ," *Ceram. Int.*, vol. 47, no. 8, pp. 11394–11404, Apr. 2021, doi: 10.1016/j.ceramint.2020.12.266.

- [19] S. B. Shen, J. L. Bu, L. X. Yu, Z. F. Wang, R. L. Wang, and R. S. Wang, "Effect of  $B_4C$ - $Yb_2O_3$  Compound Additive on Crystallization and Sintering of Fused Quartz Ceramic Materials," *Adv. Mater. Res.*, vol. 291–294, pp. 24–28, 2011, doi: 10.4028/www.scientific.net/AMR.291-294.24.
- [20] J. L. Bu, F. Ma, Y. H. Zhang, H. Y. Zhao, R. L. Wang, and Z. F. Wang, "Influence of Rare Earth Oxides on Crystallization Behavior and Sintering Performance of Fused Quartz Ceramic Materials," *Adv. Mater. Res.*, vol. 150–151, pp. 1782–1785, 2011, doi: 10.4028/www.scientific.net/AMR.150-151.1782.
- [21] J. L. Bu, Y. F. He, S. B. Shen, Y. J. Chen, Y. L. Gu, and Z. F. Wang, "Effect of  $B_4C$ - $Si_3N_4$  on Crystallization and Sintering of Fused Quartz Ceramic Material," *Adv. Mater. Res.*, vol. 1004–1005, pp. 401–404, 2014, doi: 10.4028/www.scientific.net/AMR.1004-1005.401.
- [22] S. B. Shen, J. L. Bu, L. X. Yu, J. X. Chen, and Z. F. Wang, "Study on Sintering Properties and Crystallization of Fused Quartz Ceramic Materials Containing  $BN$ - $B_4C$ ," *Appl. Mech. Mater.*, vol. 217–219, pp. 43–46, 2012, doi: 10.4028/www.scientific.net/AMM.217-219.43.
- [23] R. J. Bell and P. Dean, "The structure of vitreous silica: Validity of the random network theory," *Philosophical Magazine*, vol. 25, no. 6, pp. 1381–1398, 1972.
- [24] W. Yan, M. Wang, J. Xiao, J. Wang, and F. Xia, "Influence of  $B_4C$  Additive on Sintering and Crystallization of Fused Silica Ceramics," *Chinas Refract.*, vol. 22, no. 1, pp. 27–31, 2013.
- [25] A. A. K. Al-Hasnawi and I. A. D. Al-Hydary, "The devitrification kinetics of transparent silica glass prepared by gel-casting method," *Matér. Rio Jan.*, vol. 24, p. e, May 2019, doi: 10.1590/S1517-707620190001.0654.
- [26] J. Rivera *et al.*, "Tunable Mechanical Responses of Architected Boron Carbide-Aluminum Lattice Composites Fabricated Via Reactive Metallic Infiltration of Hierarchical Pore Structures." Rochester, NY, Jun. 12, 2023. doi: 10.2139/ssrn.4476007.
- [27] A. Wat *et al.*, "Synthesis of nanograined zirconium diboride microsphere powder feedstock via emulsification of suspensions," *Ceram. Int.*, vol. 48, no. 16, pp. 22664–22671, Aug. 2022, doi: 10.1016/j.ceramint.2021.12.161.
- [28] F. Chabert, D. E. Dunstan, and G. V. Franks, "Cross-linked Polyvinyl Alcohol as a Binder for Gelcasting and Green Machining," *J. Am. Ceram. Soc.*, vol. 91, no. 10, pp. 3138–3146, 2008, doi: 10.1111/j.1551-2916.2008.02534.x.
- [29] R. C. Breneman and J. W. Halloran, "Kinetics of Cristobalite Formation in Sintered Silica," *J. Am. Ceram. Soc.*, vol. 97, no. 7, pp. 2272–2278, 2014, doi: 10.1111/jace.12889.
- [30] R. W. G. Wyckoff, "Crystal structure of high temperature cristobalite," *Am. J. Sci.*, vol. s5-9, no. 54, pp. 448–459, Jun. 1925, doi: 10.2475/ajs.s5-9.54.448.
- [31] R. T. Downs and D. C. Palmer, "The pressure behavior of  $\alpha$  cristobalite," *Am. Mineral.*, vol. 79, no. 1–2, pp. 9–14, Feb. 1994.
- [32] S. Patnaik, "ImageJ macro to measure distance between two lines/edges," Image.sc Forum. Accessed: Sep. 18, 2023. [Online]. Available: <https://forum.image.sc/t/imagej-macro-to-measure-distance-between-two-lines-edges/42019/67>
- [33] S. Haaf, K. Dyar, A. Moore, and N. Kivi, "Devitrification Rates of Fused Silica in the Presence of Trace Impurities," *Chancell. Honors Program Proj.*, May 2016, [Online]. Available: [https://trace.tennessee.edu/utk\\_chanhonoproj/1972](https://trace.tennessee.edu/utk_chanhonoproj/1972)
- [34] N. Kivi, A. Moore, K. Dyar, and S. Haaf, "Devitrification Rates of Fused Silica in the Presence of Trace Impurities," *Chancellor's Honors Program Proj.*, May 2016, [Online]. Available: [https://trace.tennessee.edu/utk\\_chanhonoproj/1972](https://trace.tennessee.edu/utk_chanhonoproj/1972)

- [35] F. E. Wagstaff, "Crystallization Kinetics of Internally Nucleated Vitreous Silica," *J. Am. Ceram. Soc.*, vol. 51, no. 8, pp. 449–453, 1968, doi: 10.1111/j.1151-2916.1968.tb11917.x.
- [36] M. Avrami, "Kinetics of Phase Change. I General Theory," *J. Chem. Phys.*, vol. 7, pp. 1103–1112, Dec. 1939, doi: 10.1063/1.1750380.
- [37] A. Jain and S. Anthonysamy, "Oxidation of boron carbide powder," *J. Therm. Anal. Calorim.*, vol. 122, no. 2, pp. 645–652, Nov. 2015, doi: 10.1007/s10973-015-4818-3.
- [38] W. G. Fahrenholtz, "The ZrB<sub>2</sub> Volatility Diagram," *J. Am. Ceram. Soc.*, vol. 88, no. 12, pp. 3509–3512, 2005, doi: 10.1111/j.1551-2916.2005.00599.x.
- [39] Y. Q. Li and T. Qiu, "Oxidation behaviour of boron carbide powder," *Mater. Sci. Eng. A*, vol. 444, no. 1, pp. 184–191, Jan. 2007, doi: 10.1016/j.msea.2006.08.068.
- [40] G. A. Gogotsi, Ya. L. Groushevsky, O. B. Dashevskaya, Yu. G. Gogotsi, and V. A. Lavrenko, "Complex investigation of hot-pressed boron carbide," *J. Common Met.*, vol. 117, no. 1, pp. 225–230, Mar. 1986, doi: 10.1016/0022-5088(86)90037-8.
- [41] G. A. Gogotsi, Yu. G. Gogotsi, and D. Yu. Ostrovoj, "Mechanical behaviour of hot-pressed boron carbide in various atmospheres," *J. Mater. Sci. Lett.*, vol. 7, no. 8, pp. 814–816, Aug. 1988, doi: 10.1007/BF00723769.
- [42] V. A. Lavrenko, A. P. Pomytkin, P. S. Kislyj, and B. L. Grabchuk, "Kinetics of high-temperature oxidation of boron carbide in oxygen," *Oxid. Met.*, vol. 10, no. 2, pp. 85–95, Apr. 1976, doi: 10.1007/BF00614238.
- [43] V. A. Lavrenko and Yu. G. Gogotsi, "Influence of oxidation on the composition and structure of the surface layer of hot-pressed boron carbide," *Oxid. Met.*, vol. 29, no. 3, pp. 193–202, Apr. 1988, doi: 10.1007/BF00751794.
- [44] F. E. Wagstaff and K. J. Richards, "Kinetics of Crystallization of Stoichiometric SiO<sub>2</sub> Glass in H<sub>2</sub>O Atmospheres," *J. Am. Ceram. Soc.*, vol. 49, no. 3, pp. 118–121, 1966, doi: 10.1111/j.1151-2916.1966.tb15387.x.
- [45] R. Inoue, Y. Arai, Y. Kubota, Y. Kogo, and K. Goto, "Oxidation of ZrB<sub>2</sub> and its composites: a review," *J. Mater. Sci.*, vol. 53, no. 21, pp. 14885–14906, Nov. 2018, doi: 10.1007/s10853-018-2601-0.
- [46] M. M. Opeka, I. G. Talmy, and J. A. Zaykoski, "Oxidation-based materials selection for 2000C+ hypersonic aerosurfaces: Theoretical considerations and historical experience," *J. Mater. Sci.*, vol. 39, pp. 5887–5904, 2004.
- [47] W. C. Tripp and H. C. Graham, "Thermogravimetric Study of the Oxidation of ZrB<sub>2</sub> in the Temperature Range of 800° to 1500°C," *J. Electrochem. Soc.*, vol. 118, no. 7, p. 1195, Jul. 1971, doi: 10.1149/1.2408279.

## IX. Supplementary Information

### Investigation of B<sub>4</sub>C for inhibiting crystallization in silica at high temperatures

Isabel R. Crystal<sup>1,a</sup>, Ben Schauer<sup>1,a</sup>, Elizabeth Sobalvarro Converse<sup>a</sup>, James T. Cahill<sup>a</sup>, Wyatt L. Du Frane<sup>a</sup>, Gabriella King<sup>a,\*</sup>

<sup>a</sup>Materials Science Division, Lawrence Livermore National Laboratory, Livermore, CA, 94550, USA

\*Corresponding author: [king112@llnl.gov](mailto:king112@llnl.gov)

<sup>1</sup>Isabel R. Crystal and Ben Schauer contributed equally to this article.

#### Supplementary Information

This work was performed under the auspices of the U.S. Department of Energy by Lawrence Livermore National Laboratory under Contract DE-AC52-07NA27344. Released under LLNL-JRNL-854285.

This research was developed with funding from the Defense Advanced Research Projects Agency (DARPA). The views, opinions and/or findings expressed are those of the authors and should not be interpreted as representing the official views or policies of the Department of Defense or the U.S. Government. Distribution A: Approved for Public Release, Distribution Unlimited.

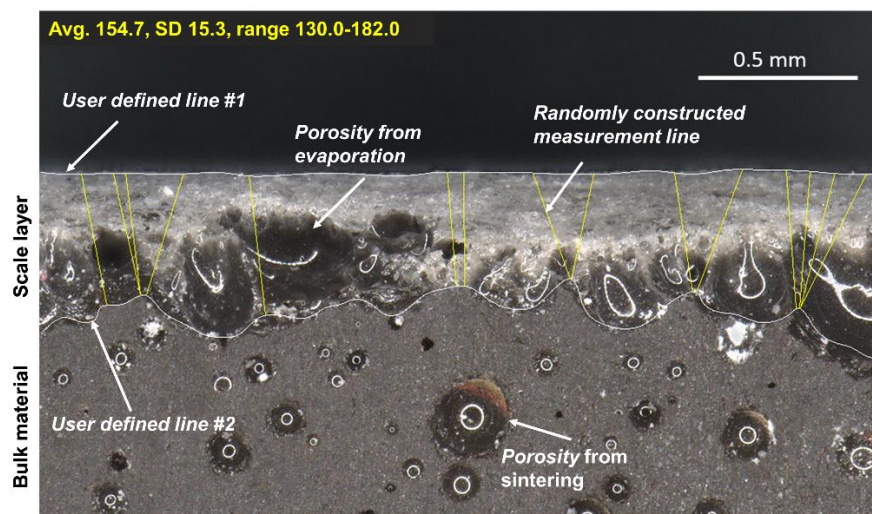


**Figure S9.** Example of an ImageJ macro used to measure the distance between two lines to determine the average scale layer thickness in for each isothermal condition, with the macro generating the yellow lines and statistics in units of pixels (in yellow) [1]. Microstructural features are shown with the white and black text but are not a result of the macro.

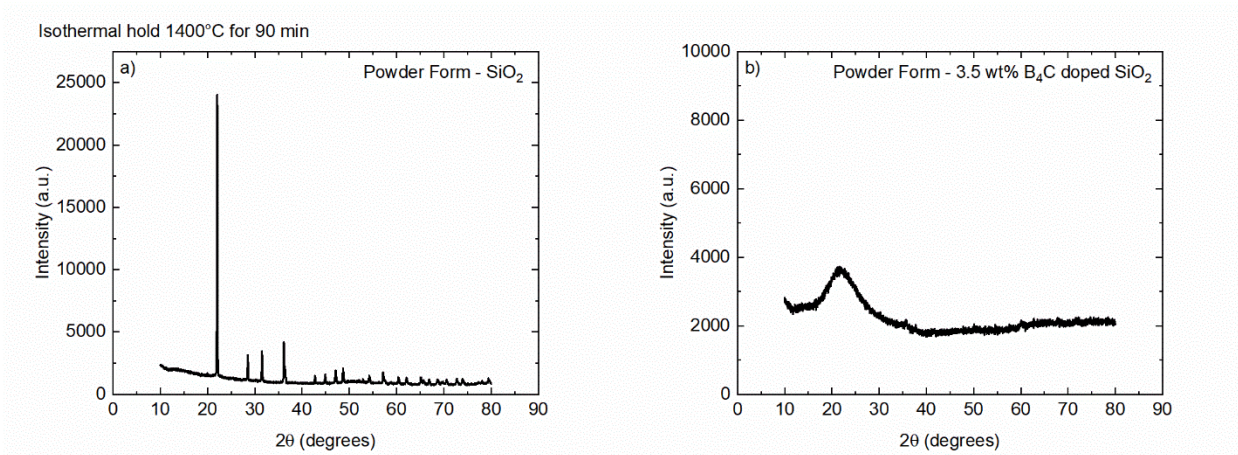


**Figure S10.** X-ray diffraction pattern for a) 0 wt% B<sub>4</sub>C powders and b) 3.5 wt% B<sub>4</sub>C doped SiO<sub>2</sub> powders subjected to the same isothermal treatment of 1400 °C for 90 minutes.

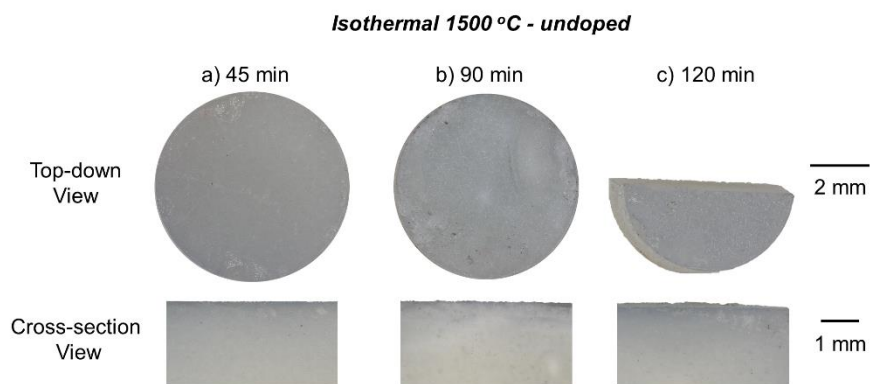


**Figure S11.** Optical microscopy of 0 wt% B<sub>4</sub>C doped gel-cast components top-down view and cross-sections at different times for the 1500 °C isothermal treatment where each time/ temperature combination is represented by a unique sample. The following treatments are imaged: a) 45 min, b) 90 min, c) 120 min at 1500 °C where the 120 min sample is not a complete cylinder as it was cross-sectioned prior to imaging the top-down surface.

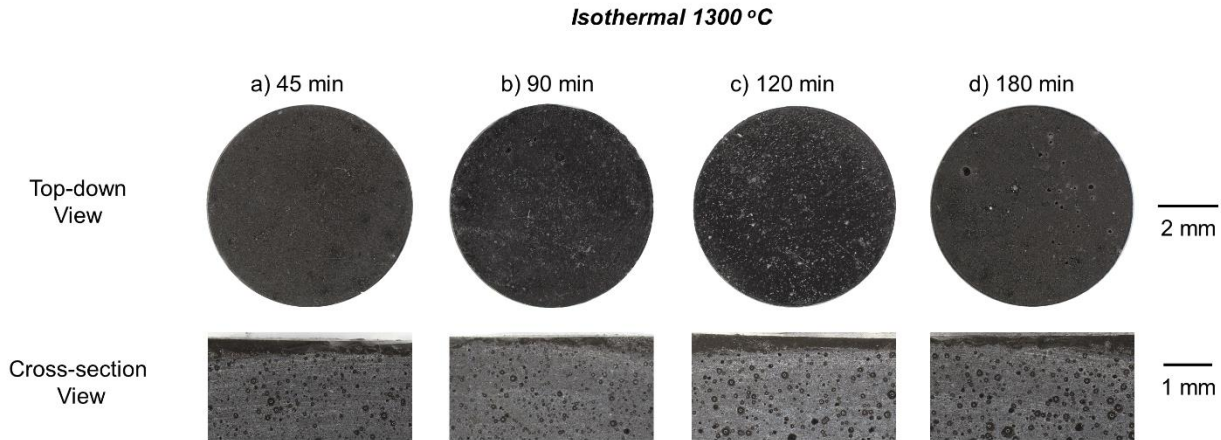


**Figure S12.** Optical microscopy of 0 wt% B<sub>4</sub>C doped gel-cast components top-down view and cross-sections at different times for the 1500 °C isothermal treatment where each time/ temperature combination is represented by a unique sample. The following treatments are imaged: a) 45 min, b) 90 min, c) 120 min at 1500 °C where the 120 min sample is not a complete cylinder as it was cross-sectioned prior to imaging the top-down surface.

- [1] S. Patnaik, "ImageJ macro to measure distance between two lines/edges," Image.sc Forum. Accessed: Sep. 18, 2023. [Online]. Available: <https://forum.image.sc/t/imagej-macro-to-measure-distance-between-two-lines-edges/42019/67>